# The Scatter in Tropical Average Precipitation Anomalies*

HUI SU AND J. DAVID NEELIN

*Department of Atmospheric Sciences, and Institute of Geophysics and Planetary Physics, University of California, Los Angeles, Los Angeles, California*

(Manuscript received 1 April 2003, in final form 11 June 2003)

ABSTRACT

Tropical mean precipitation anomalies $\langle P' \rangle$ for 3-month averages appear quite scattered in relation to tropical average sea surface temperature (SST) anomalies $\langle T_s' \rangle$, based on examination of a number of observational datasets and of atmospheric general circulation model (GCM) results. Even though SST is locally important for determining precipitation, for a given warm SST anomaly, the tropical average precipitation anomalies can be of either sign due to the near cancellation of positive against negative values. No simple relation is found between $\langle P' \rangle$ and $\langle T_s' \rangle$. On the other hand, tropical average tropospheric temperature anomalies $\langle \hat{T}' \rangle$ are approximately linearly related to SST forcing. The scatter of $\langle P' \rangle$ versus $\langle T_s' \rangle$ and $\langle \hat{T}' \rangle$ challenges the prevailing view that tropical tropospheric temperature anomalies are proportional to tropical convective heating anomalies (i.e., precipitation anomalies), while the latter are governed by SST forcing. A simple analytical model shows that convective heating anomalies are more strongly influenced by dry static-energy transports into or out of the Tropics and by nonlinearities within the Tropics than are the tropospheric temperature anomalies. As convection maintains a quasi balance between surface and tropospheric temperature, the tropical average convective heating (i.e., precipitation) anomalies react to oppose any processes that would tend to cool the tropical troposphere. On interannual timescales, the integral constraint on tropical average precipitation is dominated by the dry static energy transport into or out of the Tropics. Thus while tropical average tropospheric temperature is closely related to SST, tropical–midlatitude transports can create large scatter in tropical average precipitation.

## 1. Introduction

It is well known that the interannual variability of tropical average tropospheric temperature is dominated by El Niño–Southern Oscillation (ENSO; Sun and Oort 1995; Horel and Wallace 1981; Pan and Oort 1983). To a first-order approximation, anomalies of tropical average tropospheric temperature $\langle \hat{T}' \rangle$ exhibit a linear relationship with anomalies of tropical mean sea surface temperature (SST) $\langle T_s' \rangle$. We use $\langle\ \rangle$ to denote averages over the Tropics. Unless noted otherwise, quantities hereafter refer to tropical averages. Sobel et al. (2002) showed that interannual anomalies of tropical tropospheric temperature are correlated not only with SST anomalies averaged over the precipitating regions, but also with SST anomalies averaged over the entire Tropics. Su et al. (2003, hereafter SNM) examined the relationship of $\langle \hat{T}' \rangle$ and $\langle T_s' \rangle$ using observational data and model simulations driven by subregions of SST anomalies of various shapes, area, amplitude, and location. It was clearly demonstrated that linearity dominates the $\langle \hat{T}' \rangle$ relationship to $\langle T_s' \rangle$, regardless of the configurations of SST anomalies. On the other hand, tropical average precipitation anomalies $\langle P' \rangle$ bear a different relation to tropical mean SST anomalies, as shown in Fig. 10b of SNM. The $\langle P' \rangle$ appears rather scattered with respect to $\langle T_s' \rangle$, implying no simple relation between these two. For a given positive $\langle T_s' \rangle$, $\langle P' \rangle$ could be negative due to cancellation between positive precipitation anomalies near the origin of the SST forcing and negative anomalies surrounding it (see, e.g., SNM, their Fig. 10b). This seems contradictory to global warming scenario simulations where tropical mean precipitation increases as tropical mean SST increases (Mitchell et al. 1987; Dai et al. 2001). It also seems contradictory to a traditional view that increased SST enhances convective activity, and thus increases the precipitation rate and intensifies the hydrological cycle in the Tropics (Holton 1992). For local precipitation anomalies in the vicinity of warm SST forcing, the traditional theory certainly applies (Kiladis and Diaz 1989; Ropelewski and Halpert 1987). Why does it fail in the case of the tropical means on interannual timescales?

The scatter of $\langle P' \rangle$ versus $\langle T_s' \rangle$ was also shown in Soden (2000, his Fig. 5) for both satellite observations and climate model simulations, although only oceanic

* University of California, Los Angeles, Institute of Geophysics and Planetary Physics Contribution Number 5792.

*Corresponding author address:* J. David Neelin, Department of Atmospheric Sciences, University of California, Los Angeles, 405 Hilgard Avenue, Los Angeles, CA 90095-1565.
E-mail: neelin@atmos.ucla.edu

precipitation anomalies were included in the tropical mean. Soden pointed out that existing climate models forced by interannual SST successfully reproduced the observed tropospheric temperature variations, but the performance for tropical mean precipitation change was poor. He suggested two possible reasons: (i) the imperfection of various physical parameterization packages used in current climate models, and (ii) the inaccuracy of satellite measurements of tropical mean precipitation.

Indeed, the scatter of $\langle P' \rangle$ against $\langle T_s' \rangle$ in the satellite datasets, especially the anticorrelation of $\langle P' \rangle$ and $\langle T_s' \rangle$ in some cases, may be an indication of problems with satellite instruments or retrieval algorithms. However, the different performance of climate models in simulating the interannual variabilities of tropical mean precipitation and tropospheric temperature and drastically different behaviors of $\langle P' \rangle$ versus $\langle T_s' \rangle$ and $\langle \hat{T}' \rangle$ versus $\langle T_s' \rangle$ (SNM, their Figs. 10a,b) suggest that the dynamics and physics governing the precipitation and temperature responses to SST forcing may be fundamentally different. Su and Neelin (2002) analyzed the moisture and moist static energy budgets for anomalous subsidence forced by ENSO warm SST anomalies and found that the mechanisms for descent anomalies are quite complicated. They involve feedbacks dependent on local climatology and thus can vary from place to place, and from case to case. Considering the approximate linearity of $\langle \hat{T}' \rangle$ with $\langle T_s' \rangle$, it is not surprising that GCMs are able to capture tropospheric temperature response well but have a more difficult time reproducing precipitation response. In this study, we attempt to pinpoint the relationship between tropical mean precipitation anomaly and SST forcing using a number of precipitation datasets and compare the relationship to that of tropospheric temperature. Subsequently, with a simple analytical model, we aim to examine the physical processes involved quantitatively and thus provide insight into the dynamics governing the behavior of tropospheric temperature and precipitation response to interannual SST forcing. For present purposes, ENSO SST anomalies are discussed as a forcing to the atmosphere and model simulations with specified SST are used. We focus on the simultaneous relationship of atmospheric variables to SST at 3-month averages, noting the caveat that for some phenomena ocean–atmosphere coupling would need to be considered.

The observational datasets we choose include the monthly precipitation data from the Global Precipitation Climatology Project (GPCP; Huffman et al. 1997), and a similar satellite and rain gauge blended analysis by the Climate Prediction Center (CPC) Merged Analysis of Precipitation (CMAP; Xie and Arkin 1997). The recent precipitation data from the Tropical Rainfall Measuring Mission (TRMM) Project is also used to supplement our analysis. Besides the observational datasets, we analyze five atmospheric GCM ensemble simulations from the National Aeronautics and Space Administration (NASA) Seasonal-to-Interannual Prediction Project (NSIPP) atmospheric GCM (Bacmeister et al. 2000; Pegion et al. 2000). In contrast to the quasi-equilibrium tropical circulation model (QTCM) experiments shown in SNM (their Fig. 10b) where subregions of warm SST anomalies observed during the 1997/98 El Niño were used to force the model, the NSIPP model experiments are driven by global observed SST (Reynolds and Smith 1994). The temporal coverage of data is chosen to be from January 1982 to December 1998, which is common to most datasets. The monthly TRMM precipitation data (3B43, downloaded from the Web site http://lake.nascom.nasa.gov/data/dataset/TRMM) cover the period from January 1998 to September 2002.

This paper is organized as follows: Section 2 presents the scatterplots of tropical mean precipitation anomalies as a function of the tropical average SST anomalies for various datasets. Examples of horizontal distribution of precipitation anomalies are also shown. Section 3 describes the analytical model for the tropical mean precipitation and tropospheric temperature responses to SST forcing. In section 4, conclusions are given and an integrated view on the relationship between tropical SST, precipitation, and tropospheric temperature is proposed.

## 2. Examples of $\langle P' \rangle$ relation to $\langle T_s' \rangle$

First, we analyze the monthly precipitation data from the GPCP dataset. This global gridded precipitation analysis combines a satellite infrared estimate, microwave emission from the Special Sensor Microwave Imager (SSM/I) and in situ rain gauge measurements. Figure 1 shows the area-average precipitation anomalies within the Tropics (25°S–25°N) as a function of tropical average SST anomalies. The anomaly is relative to a climatological mean from 1982 to 1998. Both $\langle P' \rangle$ and $\langle T_s' \rangle$ are smoothed by a 3-month running mean, a typical filter for examining interannual anomalies.

It is clear that the tropical average precipitation anomalies are very scattered in relation to tropical SST anomalies. There appears to be no simple relation between $\langle P' \rangle$ and $\langle T_s' \rangle$. The linear correlation coefficient between the two variables is 0.01. The linear fit has a very small slope (0.006 mm day$^{-1}$ °C$^{-1}$). Defining $P_i'$ and $P_{Li}'$ as actual and linearly fitted precipitation anomalies at month $i$, respectively, the root-mean-square error of the linear fit, $[1/N \sum_{i=1}^{N} (P_i' - P_{Li}')^2]^{1/2}$, is 0.09 mm day$^{-1}$, which is very close to the standard deviation of the original data. For a given tropical mean SST anomaly, the tropical mean precipitation anomaly could be of either sign. For example, the $\langle T_s' \rangle$ for the period September–November 1997 is about 0.4°C, while the $\langle P' \rangle$ is close to $-0.2$ mm day$^{-1}$. In contrast, the $\langle T_s' \rangle$ for December 1997–February 1998 is 0.6°C and the $\langle P' \rangle$ is 0.05 mm day$^{-1}$. Surprisingly, the opposite signs of $\langle P' \rangle$ are associated with rather similar spatial distributions of precipitation anomalies. Figures 2 and 3 display the horizontal maps of SST, precipitation, and tropospheric

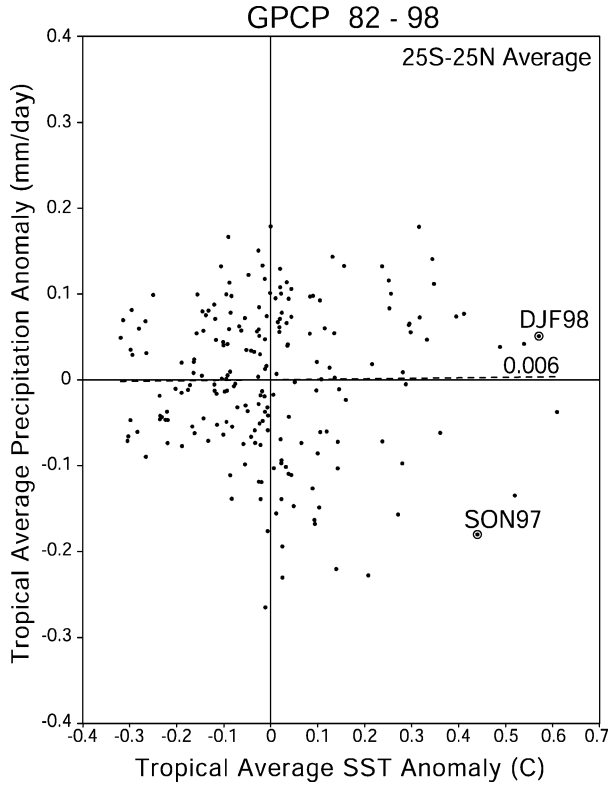


FIG. 1. Scatterplot of tropical mean (25°S–25°N) precipitation anomalies (in mm day$^{-1}$) vs tropical average SST anomalies (in °C) from Jan 1982 to Dec 1998 for the GPCP precipitation dataset. All values were smoothed using a 3-month running mean. Corresponding least squares linear fit is shown by the dashed line, with its slope marked. The two highlighted points correspond to data from Sep to Nov 1997 and from Dec 1997 to Jan 1998.

temperature anomalies for these two periods. During September–October–November (SON) 1997 and December–January–February (DJF) 1997/98, the SST anomalies are typical of a strong El Niño, with maximum anomalies concentrated in the tropical eastern Pacific. The DJF season has slightly stronger SST anomalies in the Indian and Atlantic Oceans. The precipitation anomalies are consistent with the SST anomaly distribution, with increased precipitation in the eastern and central Pacific, negative anomalies in the areas surrounding the positive anomalies, and drying in equatorial South America and Africa. The cancellation of positive anomalies by negative values makes it hard to predict the sign of tropical average precipitation anomalies by viewing the horizontal maps alone. On the other hand, the tropospheric temperature anomalies exhibit widespread warming over the entire Tropics, with maxima in the eastern Pacific. Thus the corresponding tropospheric temperature anomalies are positive in both seasons, about 0.4°C in SON and 1.1°C in DJF. This is consistent with the approximately linear relationship of tropical average tropospheric temperature anomalies with SST anomalies (see Fig. 1 in SNM).

To illustrate the similarities and differences among different algorithms for satellite data retrievals, we present another satellite rain gauge blended dataset, the CMAP precipitation, which uses similar satellite products to the GPCP. The scatterplot for the tropical average precipitation anomaly against the tropical mean SST anomaly over the period of 1982–98 is shown in Fig. 4. The precipitation data are displayed as 3-month averages. Similar to the GPCP data, the scatter of $\langle P' \rangle$ is prominent. The linear fit to the plot has a negative slope ($-0.26$ mm day$^{-1}$ °C$^{-1}$). The rms error of the linear fit is 0.11 mm day$^{-1}$, close to the rms of the precipitation variance, 0.12 mm day$^{-1}$. Hence, the linear fit is not representative of the relationship between $\langle P' \rangle$ and $\langle T_s' \rangle$. The linear correlation coefficient between the CMAP precipitation and SST anomalies is $-0.38$.

A more recent satellite precipitation estimate, the TRMM precipitation array, is regarded as a more accurate measurement than its predecessors due to its utilization of rain radar in addition to microwave radiometer and infrared instruments on board the TRMM and other satellites. It provides tropical precipitation coverage beginning in January 1998. Figure 5 shows tropical average precipitation anomalies from the TRMM-based 3B43 merged data set for the period of January 1998–September 2002. During this interval, the La Niña of 1998–2000 and the El Niño of 2002 occurred, providing a modest but reasonable range of SST anomalies. Again, the plot exhibits a negative slope ($-0.2$ mm day$^{-1}$ °C$^{-1}$) among considerable scatter. The linear correlation of the TRMM precipitation with $\langle T_s' \rangle$ is $-0.52$.

Given the differences in the plots of $\langle P' \rangle$ versus $\langle T_s' \rangle$ for satellite products, one potential hypothesis would be that the algorithms for the precipitation product require revision. It is possible that the observational dataset lacks constraints in the moisture budget, so the tropical mean precipitation values may be inconsistent with mass conservation. Hence, we extended our analysis to atmospheric GCM results that have a consistent moisture budget. Five GCM simulations with different initial conditions from the NSIPP ensemble experiments are chosen. Only the results from 1982–98 are used for comparison to other datasets. Figure 6a shows the scatterplot of $\langle P' \rangle$ versus $\langle T_s' \rangle$ for all five runs. Both $\langle P' \rangle$ and $\langle T_s' \rangle$ are smoothed by a 3-month running mean. It is evident that the tropical mean precipitation anomalies have a large scatter and poor correlation with tropical average SST anomalies for all runs. The standard deviations of $\langle P' \rangle$ for individual runs are around 0.05 mm day$^{-1}$ °C$^{-1}$. When the ensemble average is taken, the standard deviation of $\langle P' \rangle$ is 0.04 mm day$^{-1}$ °C$^{-1}$, 20% smaller than individual runs. Averaging over an ensemble of five is not sufficient to reduce transient variability in the simulated $\langle P' \rangle$. A linear fit to all values of $\langle P' \rangle$ is shown by the dashed line, with a positive slope of 0.07 mm day$^{-1}$ °C$^{-1}$. The slopes of linear fits to individual runs range from 0.05 to 0.08 mm day$^{-1}$ °C$^{-1}$. However, the rms errors of the linear fits are very close

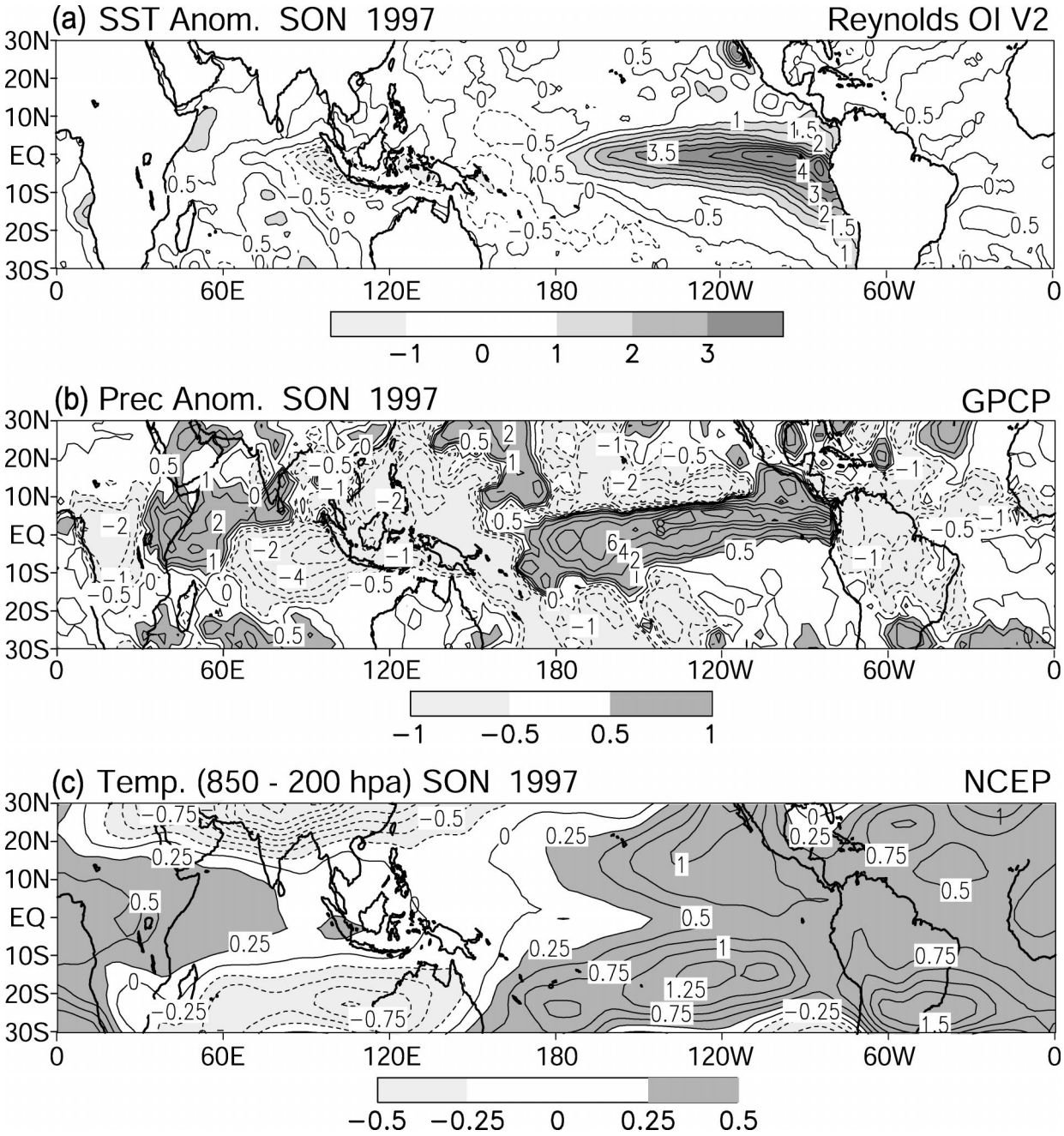


FIG. 2. Spatial patterns of observed (a) SST anomalies, (b) precipitation anomalies from the GPCP data, and (c) tropospheric temperature (850–200 mb) anomalies for the NCEP–NCAR reanalysis from Sep to Nov 1997.

to the standard deviations of $\langle P' \rangle$. Thus a linear fit to $\langle T_s' \rangle$ explains little of the $\langle P' \rangle$ behavior. The linear correlation of $\langle P' \rangle$ to $\langle T_s' \rangle$ is only 0.01.

In contrast, the tropical averaged tropospheric temperature anomalies are strikingly linear with respect to the tropical mean SST forcing. Figure 6b shows the scatterplot of $\langle \hat{T}' \rangle$ versus $\langle T_s' \rangle$ for the five AGCM experiments. The approximate linearity is prominent, with a relatively large departure from linearity occurring at large warm SST anomalies. The slope of the linear fit to all data is about 1.76°C °C$^{-1}$, slightly higher than values obtained from observational estimates of $\langle \hat{T}' \rangle$, such as the microwave sounding unit (MSU) data and the National Centers for Environmental Prediction–National Center for Atmospheric Research (NCEP–NCAR) reanalysis, which are close to 1.4°C °C$^{-1}$ (Fig. 1 in SNM). The correlation of $\langle \hat{T}' \rangle$ to $\langle T_s' \rangle$ is 0.91 in Fig. 6b. The corresponding correlation of $\langle \hat{T}' \rangle$ to $\langle T_s' \rangle$ from

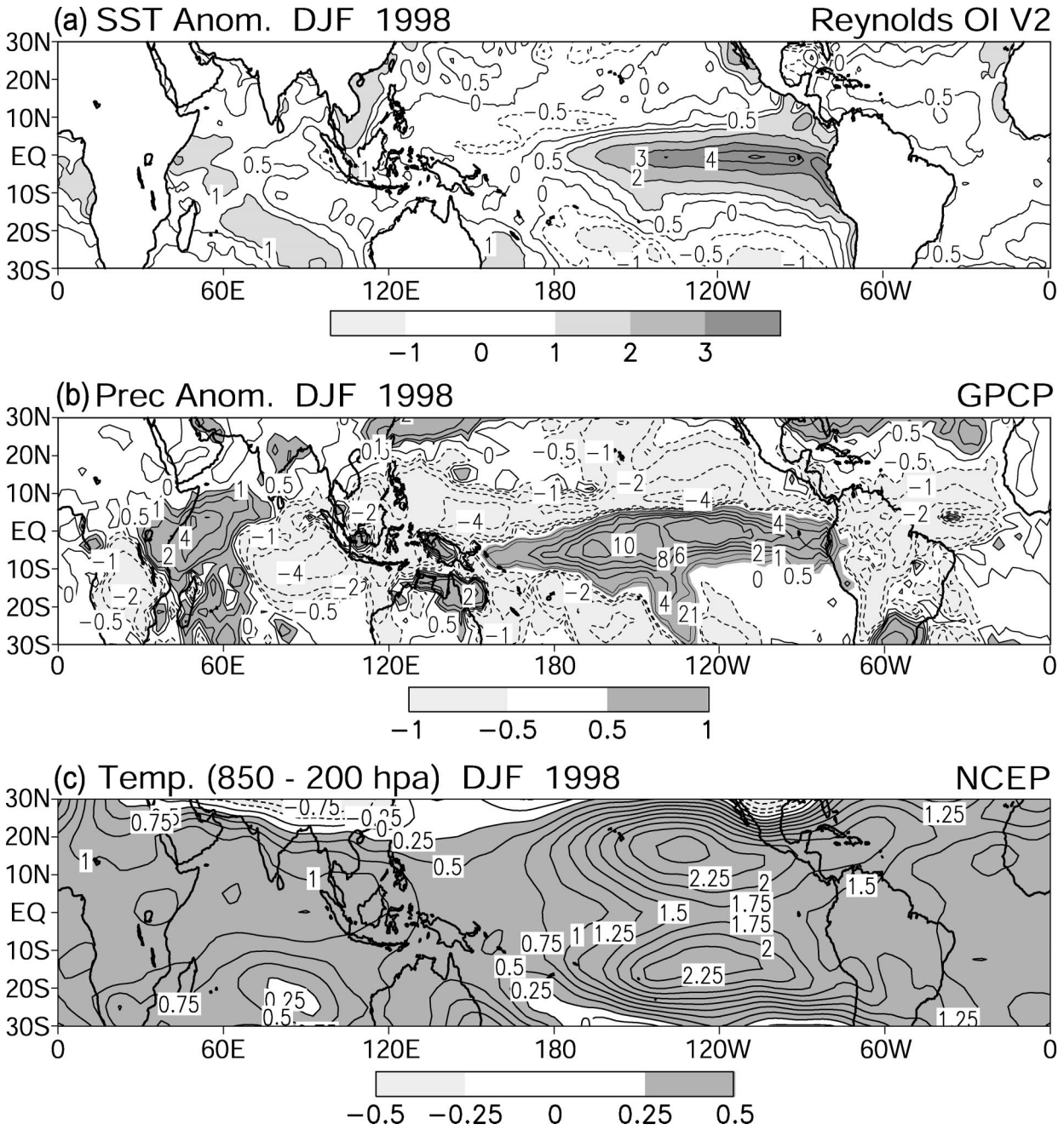


FIG. 3. Same as in Fig. 2 but for Dec 1997–Jan 1998.

the MSU and the NCEP–NCAR reanalysis is 0.80 and 0.77, respectively.

Because the scatter in tropical mean precipitation anomalies is common in all datasets and GCM simulations, it appears that this is not an artifact of observational error or imperfect numerical models. We conjecture that it is an inherent feature of the moist convective response to tropical SST forcing and other factors. In the next section, a simple model based on the equations of the QTCM (Neelin and Zeng 2000) is used to illustrate the dynamics governing the tropical mean precipitation and temperature variations.

## 3. Analytical considerations for the relationship of $\langle P' \rangle$, $\langle \hat{T}' \rangle$, and $\langle T_s' \rangle$

### *a. Derivations*

Considering a steady-state atmospheric response to SST forcing, we write the column-averaged temperature and moisture perturbation equations as follows:

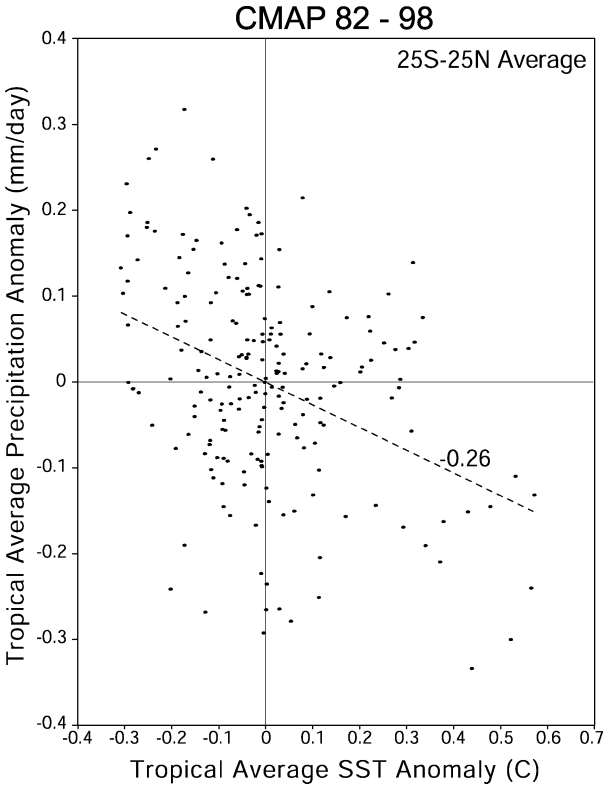


FIG. 4. Scatterplot of tropical mean (25°S–25°N) precipitation anomalies (in mm day$^{-1}$) vs tropical average SST anomalies (in °C) from Jan 1982 to Dec 1998 for the CMAP precipitation dataset. All values were smoothed using a 3-month running mean. Corresponding least squares linear fit is shown by the dashed line, with its slope marked.

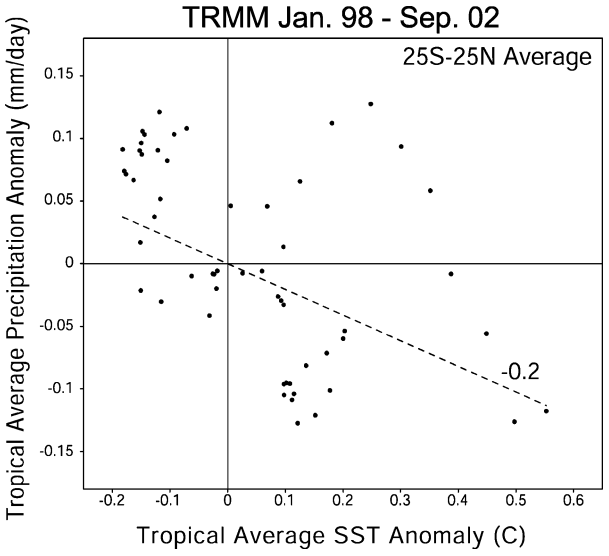


FIG. 5. Same as in Fig. 4 but for the TRMM precipitation from Jan 1998 to Sep 2002.

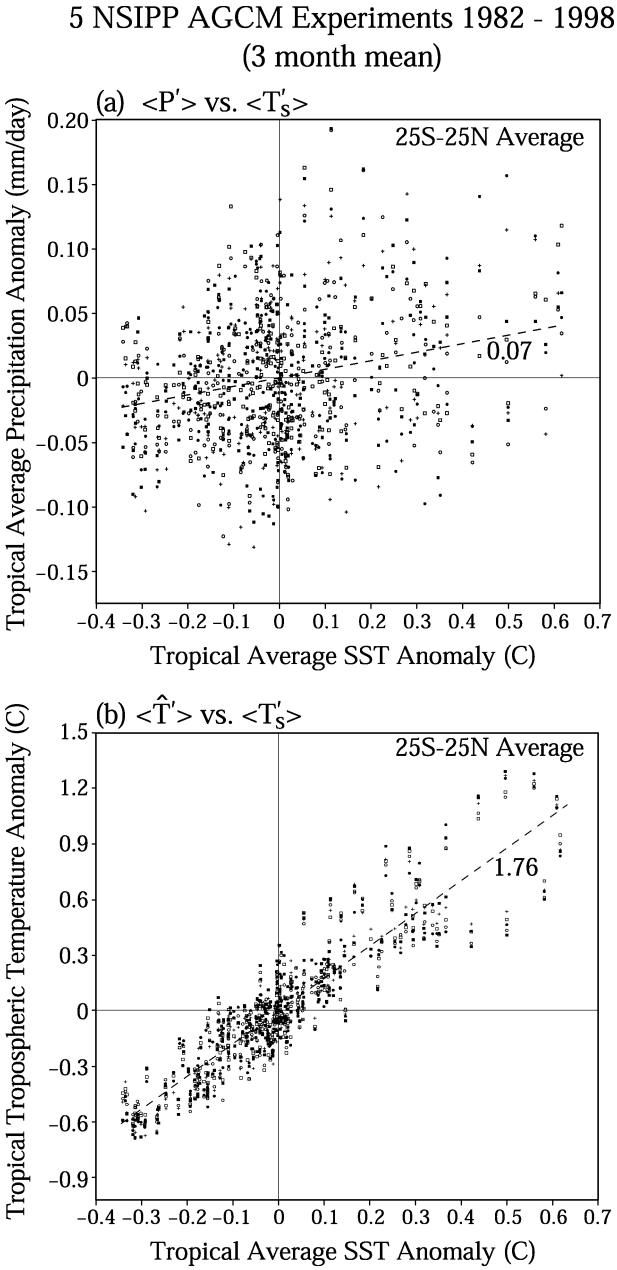


FIG. 6. Scatterplot of tropical mean (25°S–25°N) (a) precipitation anomalies (in mm day$^{-1}$) and (b) tropospheric temperature (850–200 mb) anomalies (in °C) as a function of tropical average SST anomalies (in °C) from 1982 to 1998 for the five NSIPP AGCM ensemble simulations. Corresponding least squares linear fits are shown by dashed lines, with slopes marked (units of mm day$^{-1}$ °C$^{-1}$ and unitless, respectively).

$$D'_T = \hat{Q}'_c + F'_{\text{rad}} + H' \tag{3.1}$$

$$-D'_q = \hat{Q}'_q + E', \tag{3.2}$$

where $D_T$ and $-D_q$ are the horizontal divergences of the vertically integrated dry static energy and moisture transports by the dynamics. The signs are chosen because the two tend to cancel on the tropical average.

Using $\langle\ \rangle$ to denote the averages over the whole tropical band, we define $F'_T = \langle D'_T \rangle$ and $F'_q = \langle D'_q \rangle$, where $F'_T$ and $F'_q$ are the anomalous dry static energy and moisture fluxes across the boundaries (25°S–25°N) between the Tropics and midlatitudes, respectively. Positive values of $F'_T$ mean export of energy out of the Tropics. For $F'_q$, export of moisture out of the Tropics corresponds to negative values. The anomalous moist static energy transport from the Tropics, given by $F'_T - F'_q$, is usually less than the individual terms. The atmospheric column radiative heating rate is denoted as $F_{\text{rad}}$. The surface sensible and latent heat fluxes are $H$ and $E$. The column-averaged convective heating and moisture sink are $\hat{Q}_c$ and $\hat{Q}_q$, respectively, and they satisfy

$$-\hat{Q}_q = \hat{Q}_c = P, \tag{3.3}$$

where $\hat{}$ denotes vertical averaging over the troposphere and $P$ is the precipitation rate. The $(\,)'$ indicates perturbations relative to climatological means. All quantities are in energy units.

Combining (3.1) and (3.2), we obtain the moist static energy perturbation equation

$$F'_{\text{rad}} + H' + E' = D'_T - D'_q. \tag{3.4}$$

Similar to SNM, the flux balance can be approximated as linear functions of atmospheric temperature, moisture, and SST. For simplicity, we neglect sensible heat flux anomalies and radiative flux anomalies due to atmospheric moisture changes because they are relatively small, compared to latent heat flux anomalies and radiative flux anomalies due to atmospheric temperature changes. The evaporation anomalies are parameterized using the conventional bulk-aerodynamic formula. The evaporation anomaly due to changes in wind speed is not easily linearized, so it is denoted as $\tilde{E}$. All other nonlinear effects in the fluxes can be incorporated into $\tilde{E}$. The cloud–radiative forcing amounts to roughly 10% of the surface heat flux forcing and is omitted here. Thus, we have

$$-\epsilon_T \hat{T}' + \epsilon_{T_s} T'_s + \epsilon_H(\gamma T'_s - q'_a) + \tilde{E} = D'_T - D'_q. \tag{3.5}$$

In (3.5), $\hat{T}'$ represents the tropospheric temperature anomalies and $T_s$ and $q_a$ are sea surface temperature and near-surface air moisture (in kelvins). The constants $\epsilon_T$ and $\epsilon_{T_s}$ are proportionality coefficients for atmospheric radiative heating-rate dependence on temperature and SST anomalies, with $\epsilon_T \approx 6$ W m$^{-2}$ K$^{-1}$ and $\epsilon_{T_s} \approx 6$ W m$^{-2}$ K$^{-1}$. We use $\epsilon_H = \rho_a C_H V_s$, where $\rho_a$ is surface air density and $C_H$ is the drag coefficient. The surface wind speed is denoted as $V_s$. For a tropical mean wind speed of 5 m s$^{-1}$, the value of $\epsilon_H$ is around 5. The surface saturation moisture $q_{\text{sat}}$ is a function of SST, with the dependence of $\gamma = (dq_{\text{sat}}/dT)_{T_s}$. Because the value of $\gamma$ is nearly constant in the normal range of observed SST variations, we use $\gamma \approx 3$ K K$^{-1}$, corresponding to an SST of 300 K.

When the tropical average of Eq. (3.5) is considered, the tropical mean moisture change can be related to the tropical mean tropospheric temperature variations due to the constraint on large-scale circulation by deep convection. In other words, convection vigorously adjusts tropospheric temperature to a value set by boundary layer moist static energy, which is largely determined by surface air moisture. Outside the region of deep convection, tropospheric temperature is not strongly tied to boundary layer moisture. However, the fraction of nonprecipitating regions in the Tropics is quite small. So we can approximately write $\langle q'_a \rangle \approx \gamma n \langle \hat{T}' \rangle + \xi$. The perturbation term $\xi$ indicates the contribution to tropical average moisture change not directly related to tropospheric temperature change, such as that over the nonprecipitating regions. Its effect can be incorporated into $\tilde{E}$ in (3.5), so it is omitted hereafter. The parameter $n$ is a scale factor, considering the boundary layer subsaturation and the ratio of surface air temperature to the tropospheric average temperature. The value of $\gamma n$ is 1.73 for the NSIPP model results, based on the linear regression of $\langle q'_a \rangle$ to $\langle \hat{T}' \rangle$ for the period of 1982–98.

Taking the tropical average of (3.5) and rearranging it, we obtain the relationship between tropical average tropospheric temperature and SST anomalies

$$\langle \hat{T}' \rangle = [(\epsilon_{T_s} + \epsilon_H \gamma)\langle T'_s \rangle - F'_T + F'_q + \langle \tilde{E} \rangle] \times (\epsilon_T + \epsilon_H \gamma n)^{-1}. \tag{3.6}$$

Substituting (3.6) into (3.1) or (3.2), the $\langle P' \rangle$ and $\langle T'_s \rangle$ relation can thus be expressed as

$$\langle P' \rangle = [\epsilon_H \gamma(\epsilon_T - n\epsilon_{T_s})\langle T'_s \rangle + (\epsilon_H \gamma n)F'_T + \epsilon_T F'_q + \epsilon_T \langle \tilde{E} \rangle](\epsilon_T + \epsilon_H \gamma n)^{-1}. \tag{3.7}$$

Comparing (3.6) and (3.7), we notice that both $\langle \hat{T}' \rangle$ and $\langle P' \rangle$ have an approximately linear relation to $\langle T'_s \rangle$, with superimposition of nonlinear terms such as transport anomalies and contributions to evaporation anomalies by variations of wind speed. Because these tend not to be simply related to SST, they produce scatter in the relationship to $\langle T'_s \rangle$. The proportionality constant of $\langle \hat{T}' \rangle$ and $\langle T'_s \rangle$ is approximately 1.4°C °C$^{-1}$, close to what was found in SNM. The dependence of tropical mean precipitation on $\langle T'_s \rangle$ results from competing effects of column radiative cooling and surface emissive warming. The current choice of parameters yields a rate of 0.09 mm day$^{-1}$ °C$^{-1}$. However, it is possible to have negative slope of $\langle P' \rangle$ versus $\langle T'_s \rangle$ if the value of $n$ varies. For example, $n$ is generally higher when a larger area of nonprecipitation regions is involved. This could result in a negative tropical mean precipitation anomaly for a given positive SST anomaly.

Most importantly, the transport anomaly terms in (3.7) play a greater role in producing scatter in $\langle P' \rangle$ compared to the $\langle T'_s \rangle$ term than occurs in (3.6) for $\langle \hat{T}' \rangle$. Contributing to this, (i) $F'_T$ and $F'_q$ tend to cancel in

(3.6), and (ii) the $\langle T_s' \rangle$ term in (3.7) is multiplicated by a small timescale, $(\epsilon_T - n\epsilon_{T_s})$.

Let us consider a simple case in which only evaporation is taken into account as the dominant driving force for the tropical atmospheric response to $\langle T_s' \rangle$ and all other flux anomalies are neglected. In this case,

$$\langle \hat{T}' \rangle \approx \frac{\langle T_s' \rangle}{n} - (F_T' - F_q' - \langle \tilde{E} \rangle)(\epsilon_H \gamma n)^{-1} \quad (3.8)$$

$$\langle P' \rangle \approx F_T'. \quad (3.9)$$

Here, the tropical mean precipitation anomalies would be dominated by the midlatitude–tropical dry static energy transport anomalies and are not necessarily related to SST changes, while the tropospheric temperature anomalies still approximately linearly follow the SST anomalies. The scale factor $n^{-1}$ readily gives the slope of $\langle \hat{T}' \rangle$ to $\langle T_s' \rangle$, approximately 1.73, close to the slope of the linear fit for the NSIPP ensemble simulations.

### b. Testing of the dominant balance for $\langle P' \rangle$

It appears in (3.9) that the dry static energy transport anomaly between the Tropics and midlatitudes is a dominant factor in determining tropical mean precipitation variability. Since heat and moisture budgets tend not to be well closed in data such as the NCEP–NCAR reanalysis (Trenberth and Guillemot 1998; Su and Neelin 2002), we computed the dry static energy and moisture transport anomalies for one of the NSIPP ensemble experiments. We can thus test the extent to which (3.9) gives the dominant balance for interannual $\langle P' \rangle$ variations in this model. Figure 7 shows the scatterplot of $\langle P' \rangle$ against $F_T'$, both in units of W m$^{-2}$. The tropical mean precipitation anomalies follow the dry static energy transport anomalies, with a correlation coefficient of 0.8. The linear regression gives a slope of 0.74, somewhat less than the slope of 1 predicted by the simplest case (3.9). The more general case, (3.7), gives a slope of $[1 + \epsilon_T(\epsilon_H \gamma n)^{-1}]^{-1} \approx 0.6$ for the parameters given above. The slight scatter in Fig. 7 about the $F_T'$ regression line would be due to other terms in (3.7). This confirms that variations of Tropics–midlatitude transports can indeed play an important role in the variability of tropical mean precipitation anomalies. This holds for 3-month averages, as are shown here. At much longer timescales, the variations explained by random fluctuations of the transports would be smaller.

We can also verify that $F_T'$ is not closely related to $\langle T_s' \rangle$: the correlation coefficient between the two is only $-0.1$. $F_T'$ appears very scattered when plotted against $\langle T_s' \rangle$ (figure not shown). Our claim that $F_T' - F_q'$ has a smaller effect in producing scatter in $\langle \hat{T}' \rangle$ than $F_T'$ does in $\langle P' \rangle$ can be quantified by examining the standard deviations associated with each term. The standard deviation of $F_T' - F_q'$ is 1.56 W m$^{-2}$, which yields a standard deviation for $\langle \hat{T}' \rangle$ of only 0.10 K in (3.6) or 0.16 K in (3.8), compared to the standard deviation of $\langle \hat{T}' \rangle$ explained by $\langle T_s' \rangle$ of 0.25 K in (3.6) and 0.29 K in (3.8), respectively. This can be contrasted to the standard deviation of $F_T'$ of 2.15 W m$^{-2}$, which is approximately equal to that of $\langle P' \rangle$ (2.01 W m$^{-2}$). We also note that $F_q'$ has a correlation of less than 0.5 with $\langle P' \rangle$ (compared to the $F_T'$ to $\langle P' \rangle$ correlation of 0.8). So $F_T'$ is a better predictor of $\langle P' \rangle$ than $F_q'$.

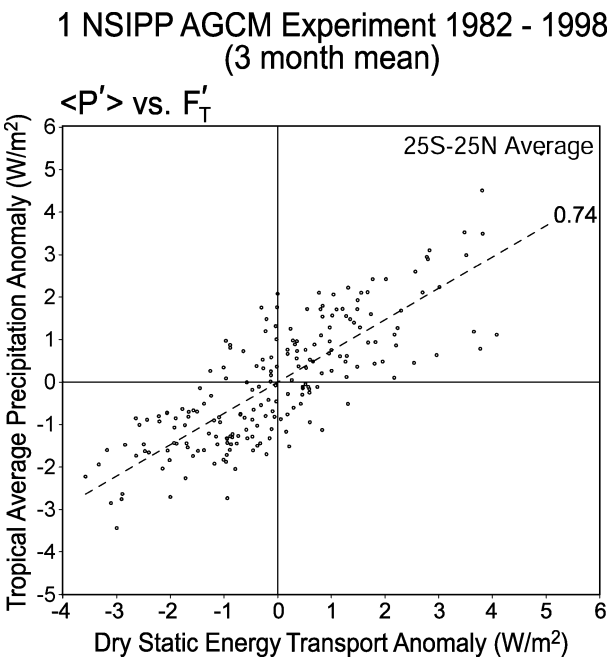


FIG. 7. Scatterplot of tropical mean (25°S–25°N) precipitation anomalies (in W m$^{-2}$) as a function of the anomalies in the export of dry static energy from the Tropics by atmospheric dynamical transports across 25°S and 25°N (in W m$^{-2}$). The results are from 1982 to 1998 for one of the NSIPP AGCM simulations. Corresponding least squares linear fit is shown by the dashed line, with its slope marked.

### c. Dynamics behind the seemingly paradoxical $\langle P' \rangle$, $\langle \hat{T}' \rangle$, and $\langle T_s' \rangle$ relations

Comparing Figs. 6a, 6b, and 7, and considering the analytical explorations in section 3a, one might ask the following questions: why does the anomalous midlatitude dry static energy transport, which appears explicitly in the temperature equation (3.1), have little effect on the tropical mean temperature, but bears a close relationship to tropical mean precipitation anomaly? Convection is known to be an active player in the chain of tropospheric response to ENSO SST forcing. Why does it not show up in the flux balance (3.5) that leads to the approximate relation between $\langle \hat{T}' \rangle$, $\langle T_s' \rangle$, and then $\langle P' \rangle$? To answer these questions, we will elaborate the dynamical processes involved in the tropospheric response to SST anomalies and associated adjustment timescales.

We consider for illustration a simple convective ad-

justment scheme in which the convective heating anomaly may be written as

$$Q_c = \begin{cases} (T^c - T)/\tau_c, & \text{if } (T^c - T) > 0 \\ 0, & \text{otherwise,} \end{cases} \quad (3.10)$$

where $T^c$ is a convective temperature profile toward which convection adjusts the temperature profile. This $T^c$ depends on the atmospheric boundary layer (ABL) moist static energy, assuming deep convection to arise out of the ABL. For the simplest case described in the previous sections, neglecting $F'_{\text{rad}}$ in (3.1), when anomalous SST occurs, boundary layer moisture $q_a$ is adjusted quickly at the timescale $(\epsilon_H \gamma)^{-1}$. This causes changes in the convective profile $T^c$, affecting convective available potential energy (CAPE). Then anomalous convection is induced to consume the perturbed CAPE and adjusts the tropospheric temperature toward $T^c$, as determined by the modified boundary layer moist static energy. The convective adjustment occurs at a fast timescale of $\tau_c$, on the order of a few hours. Although the amount of convective heating may be substantial, the change of tropospheric temperature is not dominated by convective heating, simply because of the small timescale of convective adjustment, as shown by

$$\hat{T}' = \hat{T}_c(T, q_a)' - \tau_c \hat{Q}'_c. \quad (3.11)$$

In other words, the tropospheric temperature anomalies are mainly related to boundary layer moist static energy anomalies, rather than to $\hat{Q}'_c$, due to the small value of $\tau_c$. We note the caveat that this may not hold as cleanly in observations as in the simple illustration scheme (3.10). However, Brown and Bretherton (1997) have shown such a relation tends to hold on monthly to interannual timescales from data, and SNM show it can produce the observed $\langle \hat{T}' \rangle$ and $\langle T'_s \rangle$ relation in a modeling context. The association of the tropospheric temperature and ABL moist static energy via convection is a two-way connection: Chiang and Sobel (2002) demonstrate in a column model that specified tropospheric warming can induce ABL changes.

On the tropical average, the mean convective heating (and thus precipitation) anomalies are balanced by dry static energy transport anomalies between the Tropics and midlatitudes, as shown in (3.9). The dry static energy transport, which has a large contribution from midlatitude transients, thus yields significant scatter in the tropical mean precipitation anomalies with respect to SST anomalies.

For a more general case considering radiative fluxes, the tropical mean convective heating anomaly is subject to the balance among anomalous midlatitude–tropical dry static energy transport, radiative cooling, and surface emission

$$\langle \hat{Q}'_c \rangle = F'_T + \epsilon_T \langle \hat{T}' \rangle - \epsilon_{T_s} \langle T'_s \rangle. \quad (3.12)$$

The approximate linear relationship between radiative fluxes and $\langle \hat{T}' \rangle$ or $\langle T'_s \rangle$ gives some degree of linearity for the relation of $\langle P' \rangle$ to $\langle T'_s \rangle$ or $\langle \hat{T}' \rangle$. However, because the timescales associated with radiative fluxes ($\epsilon_T^{-1}$ or $\epsilon_{T_s}^{-1}$) are relatively slow, it is efficient for $F'_T$ to create a large scatter in $\langle P' \rangle$.

TABLE 1. Adjustment timescales associated with the key dynamic processes involved in the tropical tropospheric temperature and precipitation response to SST forcing.

| | Characteristic parameter | Timescale |
|---|---|---|
| Evaporation | $(\epsilon_H \gamma)^{-1}$ | 5 days (fast) |
| Convection | $\tau_c$ | 2 h (fast) |
| Wave dynamics | L °C$^{-1}$ | 5–30 days (scale dependent) |
| Radiation | $\epsilon_T^{-1}$ | 15 days (slow) |

Therefore, convection is important in communicating upward the boundary layer anomalies, induced by SST change, to the whole troposphere. However, the amount of convective heating is not essential in the temperature response due to the small convective timescale. On the other hand, the tropical mean convective heating anomalies must come into balance with various cooling mechanisms, such as energy export to midlatitude and radiative cooling. For tropical average tropospheric temperature anomalies, the magnitude of anomalous transport of moist static energy is much smaller than that of forcing from the boundary layer on a relatively fast timescale $(\epsilon_H \gamma)^{-1}$, thus the scatter of $\langle \hat{T}' \rangle$ versus $\langle T'_s \rangle$ is small. For tropical mean precipitation anomalies, the dry static energy transport anomalies are competing against relatively small damping rates associated with radiation, and therefore, transport anomalies are able to create large scatter in $\langle P' \rangle$ versus $\langle T'_s \rangle$.

Another important physical process active in the tropical atmospheric response to SST forcing is wave dynamics, which spreads anomalies horizontally by inducing adiabatic warming in regions not directly heated to create a widespread temperature anomaly. The corresponding timescale is typical of tropical moist Kelvin or Rossby waves propagating across the domain, at phase speeds on the order of 10 m s$^{-1}$. For the tropical band, this yields a timescale of 1 or 2 months. This wave dynamics timescale does not appear explicitly in the analysis using the tropical average response, but is important to the large scale of the $\langle \hat{T}' \rangle$ signal.

Table 1 summarizes the adjustment timescales involved in the tropical atmospheric response to SST forcing. The fast boundary layer flux adjustment and convective adjustment timescales strongly link SST, boundary layer flux, and moisture to tropospheric temperature change, while the wave dynamics effectively spread the temperature anomaly over the entire Tropics. The radiative cooling (heating) due to temperature warming (cooling) acts as a relatively slow damping on the temperature variations. Among these dynamics processes, the amount of tropical averaged convective heating, that is, $\langle P' \rangle$, is subject to the balance of various mechanisms. These include dry static energy transport, the opposing

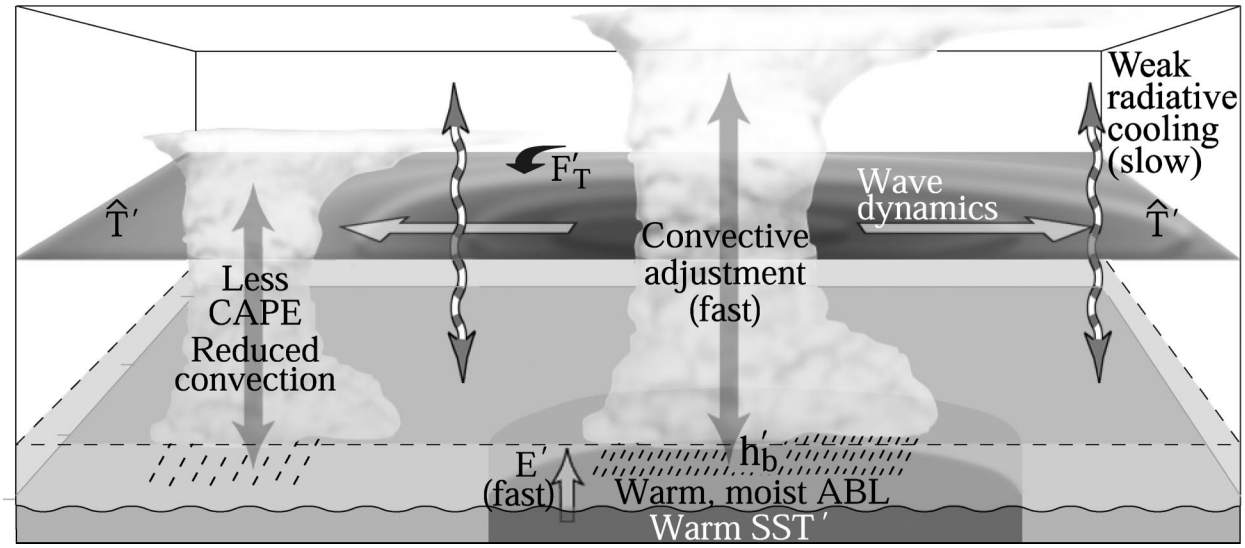


FIG. 8. Schematic of the dynamic processes involved in the tropical tropospheric temperature and precipitation response to SST forcing.

effects on evaporation due to warmer SST and higher atmospheric temperature and moisture, and to a lesser extent, moisture transport and the effect of wind speed anomalies on evaporation, and other nonlinear effects. Hence, the tropical average tropospheric temperature anomaly is predominantly governed by an approximately linear relation to tropical SST anomaly, while the tropical mean precipitation anomaly shows a great scatter in relation to SST changes and is largely balanced with anomalous dry static energy transport between the Tropics and midlatitudes.

## 4. Conclusions: An integrated view of the tropical temperature and precipitation relationship to SST

The tropical mean precipitation anomalies $\langle P' \rangle$ exhibit a great scatter in relation to tropical average SST anomalies $\langle T_s' \rangle$. Linear fits to the observational datasets and results from atmospheric GCM simulations show a wide range of slopes of $\langle P' \rangle$ versus $\langle T_s' \rangle$, and the errors of the linear fits are comparable to the standard deviations of the datasets themselves. Although it is possible that the scatter of $\langle P' \rangle$ relative to $\langle T_s' \rangle$ may be due to errors in the algorithms for the satellite precipitation products or problems with physical parameterizations used in GCMs, we propose that there is a dynamical explanation for the scatter. A simple analytical model considering the dominant balances in tropical atmospheric response to SST forcing suggests that the scatter of $\langle P' \rangle$ against $\langle T_s' \rangle$ is associated with dry static energy transport anomalies between the Tropics and midlatitudes ($F_T'$), changes in evaporation due to wind speed variations, and other nonlinear effects. In contrast, the effects of anomalous midlatitude–tropical transports and nonlinearities are secondary on the $\langle \hat{T}' \rangle$ relation to $\langle T_s' \rangle$ because of the strong linkage between SST, boundary layer moist static energy, and tropospheric temperature through boundary layer flux adjustment and tropospheric convective adjustment.

A schematic showing the dynamical processes involved in the tropical tropospheric response to SST forcing is illustrated in Fig. 8. Different arrows are used to indicate these processes, with associated timescales marked in parentheses. During an El Niño, warm SST anomalies increase surface latent heat fluxes ($E'$ in Fig. 8 with a short arrow within the boundary layer), and to a lesser extent, sensible heat fluxes and radiative flux into the atmosphere. The boundary layer moisture is increased at a relatively fast timescale. The enhanced boundary layer moist static energy ($h_b'$) changes the CAPE of the column and thus induces more vigorous convection, indicated by the long solid arrow. The fast convective timescale constrains the tropospheric temperature to a value in equilibrium with boundary layer moist static energy. Because the convection establishes this equilibrium on a relatively fast timescale, the amount of convective heating does not explicitly determine the tropospheric temperature anomaly. The tropospheric warming is spread horizontally by wave dynamics within a month or two, illustrated in the upper plane with arrows pointing outwards from the origin of the warming and gray shadings resembling propagation of warm anomalies. Hence, the entire tropical band experiences widespread warming, and the tropical average temperature anomaly is approximately linear with tropical mean SST anomaly due to the weakness of tropical averaged moist static energy transport and weak nonlinearity in the dependence of fluxes on the $\langle T_s' \rangle$ and $\langle \hat{T}' \rangle$. In this dynamical adjustment of tropospheric temperature to SST forcing, convection is an important player in communicating between boundary layer forc-

ing and deep tropospheric temperature response. Radiative cooling associated with temperature anomalies is a relatively slow damping process, depicted by curly dashed arrows.

The amount of convective heating/precipitation anomalies, on the other hand, is not simply linearly related to SST changes. Locally, near the origin of warm SST forcing, precipitation is increased. In regions away from the warm SST anomaly, increased tropospheric temperature tends to reduce CAPE unless ABL moist static energy is able to compensate. Reductions in precipitation thus tend to occur, driven by complicated mechanisms that depend on the local climatology of wind, temperature, and moisture distribution, as well as teleconnected wind and moisture changes (Su and Neelin 2002). Anomalous adiabatic warming associated with the anomalous subsidence is balanced by local cooling mechanisms such as cold or dry advection. The warming and moistening of surface air counteracts the increase in evaporation due to warmer SST, allowing other nonlinear processes to affect the tropical mean precipitation changes. For example, anomalous dry static energy import into the Tropics $F'_T$, indicated as a dark arrow in Fig. 8, is mainly due to transient eddy activity. This may increase tropospheric temperature and thus reduce CAPE, causing decreased convection over climatologically convecting regions. This could result in negative precipitation anomalies on the tropical average. The tropospheric temperature is less affected because of the close connection to $h'_b$, and hence to SST, while the convective heating reacts to compensate for whatever other heating or cooling effects are present.

The close relation of tropical averaged tropospheric temperature with SST variations independent of the value of tropical averaged convective heating is highly consistent with a convective quasi-equilibrium point of view. Convection establishes a link between tropospheric temperature and ABL moist static energy, which is constrained toward SST. The convective heating anomaly itself is simply a by-product that can be positive or negative depending on other terms in the temperature equation, such as random variations in midlatitude–tropical transports. When convection acts to constrain tropospheric temperature, the convective heating anomaly must react to oppose any process that would tend to cool or warm the troposphere away from balance with SST. For cases at long timescales and global space scales, such as global warming or paleoclimate applications, it is possible that the dominant cooling processes have a fairly simple relationship to tropospheric temperature, which in turn would result in precipitation having a simple relationship to SST. For the interannual variations examined here, the dominant anomalous cooling process in the tropical average is variations of the tropics-to-midlatitude dry static energy transport, which have little relationship to SST. These transport variations determine the interannual variability of tropical mean precipitation.

The low correlation of $\langle P' \rangle$ and $\langle T'_s \rangle$ for interannual variations demonstrated in several observational datasets seems counterintuitive, but the results here suggest it may simply be a manifestation of quasi-equilibrium aspects of convection combined with the effects of midlatitude–tropical transports.

*Acknowledgments.* We would like to thank M. P. Hoerling for asking us some of the questions that motivated this paper. This work was supported under National Science Foundation Grant ATM-0082529, National Oceanic and Atmospheric Administration Grant NA16-GP2003 and National Aeronautics and Space Administration Grant NA-GS-9358. Special thanks to J. E. Meyerson for graphical assistance.

## REFERENCES

Bacmeister, J., P. J. Pegion, S. D. Schubert, and M. J. Suarez, 2000: Atlas of seasonal means simulated by the NSIPP 1 Atmospheric GCM, NASA Tech. Memo. NASA/TM-2000-104505, Vol. 17, 190 pp.

Brown, R. G., and C. S. Bretherton, 1997: A test of the strict quasi-equilibrium theory on long time and space scales. *J. Atmos. Sci.,* **54,** 624–638.

Chiang, J. C. H., and A. H. Sobel, 2002: Tropical tropospheric temperature variations caused by ENSO and their influence on the remote tropical climate. *J. Climate,* **15,** 2616–2631.

Dai, A., T. M. L. Wigley, B. A. Boville, J. T. Kiehl, and L. E. Buja, 2001: Climates of the twentieth and twenty-first centuries simulated by the NCAR climate system model. *J. Climate,* **14,** 485–519.

Holton, J. R., 1992: *An Introduction to Dynamic Meteorology.* 3d ed. Academic Press, 511 pp.

Horel, J. D., and J. M. Wallace, 1981: Planetary-scale atmospheric phenomena associated with the Southern Oscillation. *Mon. Wea. Rev.,* **109,** 813–829.

Huffman, G. J., R. F. Adler, A. Chang, R. Ferraro, A. Gruber, A. McNab, B. Rudolf, and U. Schneider, 1997: The Global Precipitation Climatology Project (GPCP) combined dataset. *Bull. Amer. Meteor. Soc.,* **78,** 5–20.

Kiladis, G. N., and H. F. Diaz, 1989: Global climatic anomalies associated with extremes in the Southern Oscillation. *J. Climate,* **2,** 1069–1090.

Mitchell, J. F. B., C. A. Wilson, and W. M. Cunnington, 1987: On $CO_2$ climate sensitivity and model dependence of results. *Quart. J. Roy. Meteor. Soc.,* **113,** 293–332.

Neelin, J. D., and N. Zeng, 2000: A quasi-equilibrium tropical circulation model—Formulation. *J. Atmos. Sci.,* **57,** 1741–1766.

Pan, Y. H., and A. H. Oort, 1983: Global climate variations connected with sea surface temperature anomalies in the eastern equatorial Pacific Ocean for the 1958–73 period. *Mon. Wea. Rev.,* **111,** 1244–1258.

Pegion, P. J., S. D. Schubert, and M. J. Suarez, 2000: An assessment of the predictability of northern winter seasonal means with the NSIPP 1 AGCM, NASA Tech. Memo. NASA/TM-2000-104505, Vol. 18, 107 pp.

Reynolds, R. W., and T. M. Smith, 1994: Improved global sea surface temperature analyses using optimum interpolation. *J. Climate,* **7,** 929–948.

Ropelewski, C. F., and M. S. Halpert, 1987: Global and regional scale precipitation associated with the El Niño/Southern Oscillation. *Mon. Wea. Rev.,* **115,** 1606–1626.

Sobel, A. H., I. M. Held, and C. S. Bretherton, 2002: The ENSO signal in tropical tropospheric temperature. *J. Climate,* **15,** 2702–2706.

Soden, B. J., 2000: The sensitivity of the tropical hydrological cycle to ENSO. *J. Climate*, **13,** 538–549.

Su, H., and J. D. Neelin, 2002: Teleconnection mechanisms for tropical Pacific descent anomalies during El Niño. *J. Atmos. Sci.*, **59,** 2682–2700.

——, ——, and J. E. Meyerson, 2003: Sensitivity of tropical tropospheric temperature to sea surface temperature forcing. *J. Climate*, **16,** 1283–1301.

Sun, D. Z., and A. H. Oort, 1995: Humidity–temperature relationships in the tropical troposphere. *J. Climate*, **8,** 1974–1987.

Trenberth, K. E., and C. J. Guillemot, 1998: Evaluation of the atmospheric moisture and hydrological cycle in the NCEP/NCAR reanalysis. *Climate Dyn.*, **14,** 213–231.

Xie, P., and P. A. Arkin, 1997: Global precipitation: A 17-year monthly analysis based on gauge observations, satellite estimates, and numerical model outputs. *Bull. Amer. Meteor. Soc.*, **78,** 2539–2558.